

20-150 keV proton impact induced ionization of uracil: fragmentation ratios and branching ratios for electron capture and direct ionization

J. Tabet, S. Eden, S. Feil, H. Abdoul-Carime, B. Farizon, M. Farizon, S. Ouaskit, T.D. Märk

► **To cite this version:**

J. Tabet, S. Eden, S. Feil, H. Abdoul-Carime, B. Farizon, et al.. 20-150 keV proton impact induced ionization of uracil: fragmentation ratios and branching ratios for electron capture and direct ionization. *Physical Review A*, American Physical Society, 2010, 81, 012711 [10 p.]. 10.1103/PhysRevA.81.012711 . in2p3-00420485

HAL Id: in2p3-00420485

<http://hal.in2p3.fr/in2p3-00420485>

Submitted on 29 Sep 2009

HAL is a multi-disciplinary open access archive for the deposit and dissemination of scientific research documents, whether they are published or not. The documents may come from teaching and research institutions in France or abroad, or from public or private research centers.

L'archive ouverte pluridisciplinaire **HAL**, est destinée au dépôt et à la diffusion de documents scientifiques de niveau recherche, publiés ou non, émanant des établissements d'enseignement et de recherche français ou étrangers, des laboratoires publics ou privés.

20-150 keV proton impact induced ionization of uracil: fragmentation ratios and branching ratios for electron capture and direct ionization

J. Tabet, S. Eden¹, S. Feil, H. Abdoul-Carime, B. Farizon, M. Farizon, S. Ouaskit², and T. D. Märk³

Université de Lyon, F-69003, Lyon, France; Université Lyon 1, Villeurbanne; CNRS/IN2P3, UMR5822, Institut de Physique Nucléaire de Lyon; F-69622 Villeurbanne

Abstract

Fragmentation ratios have been measured for ionization and dissociative ionization for 20-150 keV ($0.9-2.4 v_0$) proton collisions with gas-phase uracil molecules. Through event-by-event determination of the post-collision projectile charge, it is possible for the first time for such a key biomolecule to distinguish between *electron capture (EC)* by the incident proton and *direct ionization (DI)* without projectile neutralization. While the same fragment ion groups are observed in the mass spectrum for both processes, electron capture induces dissociation with greater efficiency than direct ionization in the impact energy range of 35-150 keV ($1.2-2.4 v_0$). In this range electron capture is also less abundant than direct ionization with a branching ratio for electron capture / total ionization of < 50%. Moreover, whereas fragmentation ratios do not change with energy in case of electron capture, direct ionization mass spectra show a tendency for increased fragmentation at lower impact energies.

Key Words

Uracil, proton impact, ionization, dissociative ionization, electron capture, mass spectrometry

¹ Also of *Department of Physics and Astronomy, Open University, Walton Hall, Milton Keynes, MK7 6AA, UK*

² Permanent address: *Université Hassan II-Mohammédia, Faculté des Sciences Ben M'Sik (LPMC), B.P.7955 Ben M'Sik, Casablanca, Morocco*

³ *Institut für Ionenphysik und Angewandte Physik, Leopold Franzens Universität, Technikerstrasse 25, A-6020 Innsbruck, Austria*

1. Introduction

The exposure of living tissue to ionizing radiation can kill cells and initiate mutations or cancers, effects which have been traced to the structural and chemical modification of DNA (deoxyribonucleic acid) including strand breaks and clustered lesions [von Sonntag 1987]. In the wake of the pioneering work directly linking specific molecular-scale interactions to DNA strand breaks [e.g. Boudaiffa *et al.* 2000], the experimental and theoretical study of radiation-induced processes in isolated biomolecules has developed into a significant field at the borderline between physics, chemistry, and biology. A number of recent contributions to the subject have focused upon interactions of relevance to cancer therapy techniques in which beams of accelerated ions are used to deliver localized doses of energy to kill cells within tumors (proton and hadron therapies) [Moretto-Capelle and Le Padellec 2006]. These treatments exploit the *Bragg peak* maximum for energy deposition by incident ions at velocities around $2.0 v_0$ (100 keV for protons), this peak maximum being a product of the interplay between ionization, excitation, and charge exchange processes as the projectiles slow down in a medium [Biaggi *et al.* 1999, Cabrera-Trujillo *et al.* 2003].

Uracil ($C_4H_4N_2O_2$) is one of the four nucleobases in ribonucleic acid (RNA), the others being adenine, cytosine, and guanine. RNA plays a key role in the translation of genetic information and includes the same nucleobases as DNA except for uracil which replaces thymine; both nucleobases pair with adenine in the respective nucleic acids. While other tautomeric forms of uracil are possible, the structure shown as an insert in Fig. 1 is the only one which has been identified both in solution and in the gas phase [Marian *et al.* 2002, Becker and Kogan 1980]. The geometrical structure and conformational flexibility of uracil has been studied on the basis of MP2 and DFT calculations by Shishkin *et al.* [2003]. In addition to its important role in biosynthesis and radiobiology, uracil was chosen for the present experiments due to the relatively large volume of comparable gas-phase ionization data available already in the literature (discussed in section 3).

The present work provides for the first time fragmentation patterns (ratios) for the ionization of a nucleobase as a function of proton impact energy also allowing to distinguish between charge exchange collisions between the projectile ion and target molecule and direct ionization events in the velocity range coinciding with maximum energy deposition (Bragg peak maximum). Beyond their relevance to the development of progressively more refined mechanistic models of ion-induced radiation damage in biological materials [Friedland *et al.* 2003], the results are of fundamental interest

with respect to the production of fragment ions either by electron capture or by direct ionization in the case of an electronically and geometrically complex target molecule such as a nucleic base.

2. Experimental

The crossed-beam apparatus used for the present experiments is shown schematically in Fig. 2 [Gobet *et al.* 2001]. Pure molecular hydrogen is ionized in a standard RF-gas discharge source (80 MHz) typically operated at 30 W with a H₂ pressure of 1 Pa. Beams of singly charged ions extracted from this gas discharge ion source are accelerated to energies between 20 and 150 keV with a resolution ($\Delta E/E$) of 0.01. The accelerator system has been described in detail elsewhere [Carré *et al.* 1980]. A first magnetic sector field is used to separate protons from other ions such as H₂⁺, H₃⁺, and other ions originating from impurities in the source. After collimation by means of two circular apertures of radius 0.5 mm set 1 m apart, the proton beam is crossed at right angles with an effusive beam of uracil molecules. The uracil beam is formed by the sublimation of uracil powder (purchased from Sigma-Aldrich, minimum purity 99%) in a temperature-controlled Knudsen-type oven operated typically at 175 – 200 °C. Previous studies indicate that minimal thermal decomposition and isomerization of uracil occurs at these temperatures (Desfrancois *et al.* 1996). Accordingly, no evidence was observed for temperature-dependence in the present mass spectra for uracil ionization by proton impact. The exit aperture of the oven has a diameter of 1 mm and is positioned 2 mm below the incident proton beam in order to achieve a high-density target beam. The charge state of the projectile after a collision with an uracil molecule is determined using a second magnetic sector field mass analyzer with three channeltron detectors located at the appropriate positions to detect H⁺, H⁰, and H⁻. However, due to the low statistics for the coincident detection of an H⁻ projectile with a product ion (e.g. less than 0.2% of all coincidence events at 80 keV), double electron capture results are not presented in this paper.

A custom-built linear time-of-flight (TOF) mass spectrometer is used to analyze the uracil product ions formed by the impact of a proton with an uracil molecule. The instrument comprises an extraction region defined by parallel plates (± 150 V, 10 mm apart) on either side of the uracil beam, an acceleration region, a drift tube of 120 mm length, and a channeltron detector. The positive product ions are extracted from the interaction region perpendicularly to both the proton and uracil beam, the extraction and acceleration fields are set following the conditions defined by Wiley and McLaren [1955] in order to focus ions selected precisely at the detector entrance.

It is important that the proton projectile beam does not contain fast hydrogen atoms formed by the neutralization of protons in collisions with surfaces or the residual gas. Thus the background vacuum is maintained below 10^{-6} Torr and the alignment of the proton beam is verified prior to each experiment. Furthermore, single collision conditions are necessary to guarantee the unambiguous identification of the ionization processes. Both was checked with 80 keV protons by varying the target jet density by a factor of five changing the oven temperature accordingly. As changing the oven temperature in this way did not affect the measured branching ratio ($25.4\% \pm 2$) for electron capture (electron capture events divided by the sum of EC and DI events), it can be concluded that interactions between uracil molecules and hydrogen atoms neutralized in the jet did not contaminate the product ion signal because it is known from earlier measurements that for instance for 80 keV neutral hydrogen atom collisions with water molecules [Gobet *et al.* 2006] about 70% of the collisions led to electron loss reactions.

The time-of-flight (TOF) measurement to allow the determination of the mass-to-charge ratio (m/q in Thomson) of the product ions relies for its starting pulse on the detection of the corresponding proton projectile. As mentioned above each projectile that crosses the interaction region can be detected whatever its post-interaction charge state. The energy transfer during a collision with a target molecule is expected to be less than ~ 100 eV by analogy with Cabrera-Trujillo *et al.*'s [2000] calculations for 25 keV low-impact-parameter proton collisions with nitrogen, oxygen, and fluorine atoms. As this is small in comparison with the incident kinetic energy of the projectiles (20-150 keV), the precise time at which the proton/uracil interaction takes place can be determined for each detected projectile, and the time difference between a pulse at the product ion channeltron detector of the TOF and the proton/uracil interaction equals the flight time of the product ion. Clearly, the number of projectiles has to be sufficiently low for each product ion signal to be correlated to exactly one projectile. Therefore, only one proton is allowed to cross the interaction region during a time interval equal to twice the flight time of the heaviest conceivable product ion, that is the uracil parent ion. For the present experimental arrangement, this limits the primary ion beam current to 2000 protons per second.

By simultaneously determining the mass-per-charge ratio of the product ions and the post-interaction charge of the projectile, the experiment enables *direct ionization* (product ion detection with coincident H^+ detection after the secondary magnetic analyzer) to be distinguished from *electron*

capture (coincident product ion and H^0 detection) for each ionization event. Thus, in the present terminology, direct ionization (DI) describes the removal of an electron from the uracil molecule to the continuum, and electron capture (EC) describes the transfer of an electron from the uracil molecule to the projectile. The fragmentation and branching ratios presented in section 3 correspond to single ion production only; events involving the detection of two or more fragment ions in coincidence with a single projectile (including events involving charge transfer *and* electron emission) are thus not included. At 80 keV, double ion production represents only about 5% of all observed ionization events. Due to the relatively poor statistics, double ion production results are not discussed further in the present communication.

3. Results and Discussion

3.1 Branching ratios for electron capture and direct ionization

Fig. 1 shows ions formed by electron capture as a percentage of the total number of ions produced (that is $EC/EC + DI$). The errors for this branching ratio estimated on the basis of the variation between repeated measurements for 80-150 keV protons are approximately $\pm 2\%$. In this energy range, the projectile detection signals were sufficiently strong to be separated completely from the noise, corresponding to projectile detection efficiencies approaching 100%. The errors are larger for impact energies below 65 keV because the threshold had to be set closer to the noise level. Branching ratios for the 20 and 23 keV measurements are not included here due to large errors resulting from the low number of observed direct ionization events.

Branching ratios for electron capture in ionizing collisions with protons are available for a number of atomic and molecular targets [e.g. [Rudd *et al.* 1983](#), [Gobet *et al.* 2001](#), [Gobet *et al.* 2004](#), [Luna *et al.* 2007](#)]. In each case, the %EC decreases with increasing impact energy in the present energy range. Fig. 3 shows the present uracil results on a logarithmic impact energy scale with previous electron capture branching ratios measured for proton impact ionization of water [[Gobet *et al.* 2001](#), [Gobet *et al.* 2004](#), [Luna *et al.* 2007](#)]. It is worth noting that the branching ratios calculated (assuming negligible double ionization) from Luna *et al.*'s [[2007](#)] recent coincidence data are in good agreement with the water ionization results recorded using the present experimental system [[Gobet *et al.* 2001](#),

2004]. Fig. 3 also shows %EC calculated from Rudd *et al.*'s [1983] absolute cross sections for electron emission and total ionization in proton collisions with He, CO₂, CH₄, and O₂.

It is interesting to consider Fig. 3 in the context of the loose trend apparent in Rudd *et al.*'s data [1983] for atoms with higher ionization energies to demonstrate greater %EC in the lower energy part of the present range. In a simple Bohr-type model, this trend can be rationalized on the basis of approximate equivalent *velocities* of the bound electron and the incident proton providing favorable conditions for electron capture. As far as we are aware, no previous data is available to derive %EC values for a molecule with a similarly low ionization energy to that of uracil (IE = 9.59 ± 0.08 eV [Denifl *et al.* 2004]). However, the close agreement of the uracil data with the previous H₂O (IE = 12.65 ± 0.05 eV [Snow and Thomas 1990]) and CH₄ (IE = 12.61 ± 0.01 eV [Berkowitz *et al.* 1987]) measurements [Rudd *et al.* 1983, Gobet *et al.* 2004, Luna *et al.* 2007] indicates that the lowest ionization energy is not a sensitive determinant for the relative contributions of EC and DI in 20-150 keV proton collisions with molecules, possibly suggesting that the capture of valence electrons from orbitals other than the HOMO plays a significant role. This interpretation appears to be consistent with uracil⁺ accounting for less than 15% of the presently observed ions formed by electron capture (see section 3.2), while Denifl *et al.* [2004] reported uracil fragment ion appearance energies in the range 10.89 -14.77 eV.

3.2 Proton impact ionization mass spectra

Fig. 4 shows the mass spectrum for single ion production by electron capture and direct ionization in 80 keV (1.8 v_0) proton collisions with gas-phase uracil molecules. The histogram includes data which contributed to the summed mass spectrum for 20-150 keV (0.9-2.4 v_0) proton impact presented by Couplier *et al.* [2002]. More recently, a mass spectrum for 100 keV (2.0 v_0) proton impact ionization of gas-phase uracil has been reported by Le Padellec *et al.* [2008]. Schlathöler and co-workers studied uracil ionization in collisions with various ions, including multiply charged species. In particular, complete mass spectra were presented for He²⁺, C²⁺, N²⁺, and O²⁺ impact at 0.2 v_0 [Schlathöler *et al.* 2005], C¹⁻⁶⁺ impact at 0.4 v_0 [Schlathöler *et al.* 2005, Schlathöler *et al.* 2006, de Vries *et al.* 2004, de Vries *et al.* 2002], C⁶⁺ impact at 0.5 v_0 [Schlathöler *et al.* 2005], O⁵⁺ impact at 0.5 v_0 [Schlathöler *et al.* 2006], C⁺ impact at 0.1-0.3 v_0 [Schlathöler *et al.* 2005, de Vries *et al.* 2004], and ¹²⁹Xe¹⁴⁺ impact at 0.2 v_0 [de Vries *et al.* 2003]. The same groups of singly charged product ions were observed in these varied ion impact conditions, with the exception of Schlathöler and co-workers' He²⁺ impact result

(discussed below). Unlike the present work, the previously presented ion impact mass spectra did not separate ionization processes as a function of charge transfer between the target and the projectile.

Recent electron impact ionization studies of gas-phase uracil have been carried out at incident energies of 200 eV ($3.8 v_0$) [Coupier *et al.* 2002], 120 eV ($3.0 v_0$) [Feil *et al.* 2004], and 70 eV ($2.3 v_0$) [Denifl *et al.* 2004, Imhoff *et al.* 2007, NIST] using quadrupole mass spectrometers (QMS). Also using a QMS analyzer, Jochims *et al.* [2005] measured ion yields following 20 eV photo-ionization of uracil. For gas-phase uracil ionization, table 1 compares the present 80 keV ($1.8 v_0$) proton impact mass spectrum with Le Padellec *et al.*'s [2008] 100 keV ($2.0 v_0$) proton impact data and with the previous high-resolution electron impact and photo-ionization measurements [Imhoff *et al.* 2007, Denifl *et al.* 2004, Jochims *et al.* 2005]. The desorbed cations observed by Imhoff *et al.* [2007] following 200 eV ($0.01 v_0$) Ar^+ impact on condensed uracil are also listed in the table. With reasonable allowance for differences in resolution and background noise, peaks were generally observed at the same m/q values for the different projectiles. Similarly, whereas the relative intensities of the different ion groups differed for direct ionization and electron capture and varied to some extent with impact energy (see section 3.3), no associated variations in peak positions were observed in the present mass spectra.

The previous high-resolution electron impact, ion impact, and photo-ionization mass spectrometric studies of gas-phase uracil have shown the contributions of fragment ions of m/q close to uracil^+ to be negligible [Denifl *et al.* 2004, Feil *et al.* 2004, Imhoff *et al.* 2007, Jochims *et al.* 2005, de Vries *et al.* 2004]. Therefore, while the m/q resolution is insufficient to confirm or discount the production of intact *uracil* ions stripped of one or more exterior hydrogen atoms, it is reasonable to assume that such channels have a negligible contribution to the present data.

Fig. 4 shows that fragment ion production was significant in the m/q ranges corresponding to ions with 1-5 *heavier* (C, N, or O, as opposed to H) atoms. By contrast, ions produced by the loss of just one *heavier* atom have only been observed by 20 eV photo-ionization of gas-phase uracil (a very weak feature at 96 Thomson) [Jochims *et al.* 2005], $0.2 v_0$ He^{2+} impact on gas-phase uracil (78 and 94-96 Thomson), and 200 eV ($0.01 v_0$) Ar^+ irradiation of condensed uracil (95-97 Thomson) [Imhoff *et al.* 2007]. Jochims *et al.* [2005] and Imhoff *et al.* [2007] attributed these weak peaks to oxygen removal (combined with the possible removal of one or two hydrogen atoms) from uracil or protonated uracil, respectively. Schlathölter *et al.* [2005] rationalized the unusually strong production of fragment ions in this range following $0.2 v_0$ He^{2+} impact on the basis of the specific interplay between target and

projectile electronic levels. Although no corresponding features were observed in the present 20-150 keV (0.9-2.4 v_0) proton impact mass spectra, the count rates between 75 and 90 Thomson were slightly higher than the background noise, suggesting very weak ion production. No evidence was observed for fragment ions above 90 Thomson. The weakness of any production of ions with 6 or 7 *heavier* atoms suggests that the dissociative ionization of gas-phase uracil following proton impact occurs almost exclusively via cleavage of the central aromatic ring. Accordingly, neutral HNCO loss (a *retro Diels-Alder reaction*) has been widely recognized as the initial step in the dominant fragmentation pathways of (uracil⁺)^{*}, leading to fragment ion production with $m/q \leq 69$ Thomson. Subsequent production of HNCO, HCN, CO, and H production (as well as combinations of these neutrals) are understood to account for the lower m/q fragment ion peaks [Jochims *et al.* 2005]. It should be noted that bond rearrangements have been shown to occur prior to the fragmentation of quite similar metastable polyatomic cations to (uracil⁺)^{*} (see, for example, Imhoff *et al.*'s [2005] studies of the 70 eV electron-impact induced dissociative ionization of thymine and deuterated thymine).

The peak structure observed between 20 and 69 Thomson was in close agreement with the previous ion impact [e.g. De Vries *et al.* 2004], electron impact [e.g. Imhoff *et al.* 2007] and 20 eV photo-ionization mass spectra [Jochims *et al.* 2005]. Denifl *et al.* [2004], Imhoff *et al.* [2007], and Jochims *et al.* [2005] proposed broadly consistent assignments for the various peaks, with the notable exception of the major peak at 42 Thomson which was respectively attributed to CNO⁺, C₂H₄N⁺, and C₂H₂O⁺. Jochims *et al.* [2005] suggested that direct CNO⁺ production from uracil⁺ is unlikely as it would require the rupture of 3 bonds, while CNO⁺ loss from (C₃H₃NO⁺)^{*} would involve a complex nuclear rearrangement. However it may be countered that the C₃H₃NO⁺ - HCN → C₂H₂O⁺ channel proposed by Jochims *et al.* [2005] would also involve a fairly complex rearrangement of the metastable precursor. Imhoff *et al.* [2005] attributed C₂H₄N⁺ production to cleavage of the N1-C2 and C4-C5 bonds (see Fig. 2) combined with the translation of the H atom bonded to N3 in (uracil⁺)^{*}. Although the present work does not provide any new evidence to identify the dominant 42 Thomson fragment ion, it should be noted that higher energy transfer can be expected for 20-150 keV proton impact than for 70 eV electron impact or 20 eV photo-ionization. Indeed Moretto-Capelle and Le Padellec [2006] reported significant emission of electrons with kinetic energies up to 50 eV following 25-100 keV proton impact upon gas-phase uracil, as well as weaker emission of 50 - 200 eV electrons. Therefore ionization pathways involving high energy deposition, increasing the likelihood of multiple bond cleavage and

fragmentation prior to nuclear rearrangement, are expected to be significant in the present collision conditions. Accordingly, we suggest that the present peak at 42 Thomson may contain a relatively strong contribution of CNO^+ ions.

The 12-18 Thomson group is apparent in the electron impact measurements covering this range [Coupier *et al.* 2002, Imhoff *et al.* 2007, NIST], in the previous ion impact data [Le Padellec *et al.* 2008, Schlathölder *et al.* 2005, Schlathölder *et al.* 2006, de Vries *et al.* 2004], and in Jochims *et al.*'s [2005] photo-ionization mass spectrum. In the present data, particularly strong peaks were observed at 12 (C^+) and 14 Thomson (N^+ or CH_2^+). For 70 eV electron impact on gas-phase uracil and 200 eV Ar^+ impact on condensed uracil, Imhoff *et al.* [2007] assigned cation production in this mass range principally to CH_2^+ and CH_3^+ production. The relatively high intensity of the C^+ peak in the present mass spectra may be due to greater energy deposition by 20-150 keV proton impact leading to increased multi-fragmentation.

H^+ production was observed in the present work and in all the previous ion and electron impact measurements which covered the full product ion mass range [de Vries *et al.* 2003, de Vries *et al.* 2004, Schlathölder *et al.* 2004, Schlathölder *et al.* 2006, Coupier *et al.* 2002, Imhoff *et al.* 2007]. No evidence was observed in the present data for ion production between the strong peaks at 1 and 12 Thomson. Conversely, H_2^+ production from gas-phase uracil was observed in Imhoff *et al.*'s [2007] 70 eV ($2.3 v_0$) electron impact experiments and in diverse ion impact mass spectra reported by Schlathölder and co-workers [de Vries *et al.* 2003, de Vries *et al.* 2004, Schlathölder *et al.* 2004, Schlathölder *et al.* 2006, Coupier *et al.* 2002, Imhoff *et al.* 2007]. Indeed, the only previous mass spectrum showing the absence of H_2^+ products from gas-phase uracil was de Vries *et al.*'s [2003] electron-ion coincidence measurement for 0.2 v_0 $^{129}\text{Xe}^{14+}$ impact. To the authors' knowledge, no attempt has been made to pinpoint the dominant fragmentation pathways associated with H^+ or H_2^+ production from uracil.

The present lack of evidence for the production of *small* doubly charged ions (notably C^{2+} , N^{2+} , and O^{2+}) is consistent with Feil *et al.*'s [2004] observation of no signals of appreciable intensity for multiply charged ions following electron impact upon gas-phase uracil at energies from the ionization threshold to 1 keV ($8.6 v_0$). Accordingly, Le Padellec *et al.* [2008] commented that correlated fragment ion measurements show doubly charged nucleobase parent ions (e.g. uracil $^{2+}$) produced by proton impact to be scarce. De Vries *et al.* [2002] described the ratio of doubly to singly charged product ions

as *surprisingly low* at ~0.75% for C^{1-6+} impact at velocities in the range 0.1-0.7 v_0 , while the formation of specific multiply charged product ions has been investigated in more detail for $^{129}\text{Xe}^{5-25+}$ impact upon uracil at 0.2 v_0 [de Vries *et al.* 2003, de Vries *et al.* 2004], Xe^{8+} impact at 0.2 v_0 [Schlathölder *et al.* 2006], and $^{129}\text{Xe}^{25+}$ impact at 0.6 v_0 [Schlathölder *et al.* 2004].

3.3 Fragment ion production as a function of impact energy and ionization process (EC / DI)

The present data provides an ideal platform to compare direct ionization with electron capture in terms of the branching ratios for fragment ion production against total ionization and their variation with impact energy. Product ion branching ratios calculated separately for EC and DI (e.g. the number of product ions produced by EC in a given mass range / the total number of product ions produced by EC) are presented in Fig. 5 and table 2. The errors listed in the table are statistical ($n^{-1/2}$) and do not take into account the acceptance of the time-of-flight apparatus. Fragment ions are separated into 7 groups corresponding to the clear peaks in the mass spectra (see Fig. 4). Although the groups have been named after the ions associated with the maxima (see table 1), they include counts over the full range of each peak (e.g. 35-47 Thomson for the $\text{CNO}^+ / \text{C}_2\text{H}_4\text{N}^+ / \text{C}_2\text{H}_2\text{O}^+$ group). The contribution of background noise could be removed easily as it was observed to be constant across all flight times.

Fig. 5 and table 2 do not show any clear evidence for impact energy-dependence in the electron capture product ion branching ratios following proton collisions with gas-phase uracil. It is interesting to contrast these results with the proton - H_2O collision data recorded by Gobet *et al.* [2004] using the same apparatus. For electron capture from H_2O , the branching ratio for fragment ion production increased from 47% at 20 keV to 67% at 150 keV*. This coincided with an approximate 25-fold decrease in the total cross section for electron capture [Gobet *et al.* 2001, 2004]. Thus the observed product ion branching ratios following EC in proton - H_2O collisions were broadly consistent with the generalized association of smaller impact parameters (more *direct* collisions, smaller cross sections) with greater energy deposition and increased fragmentation [Walch *et al.* 1994, Cabrera-Trujillo *et al.* 2000]. The cross sections for EC in proton - uracil collisions also decrease significantly from 20 to 150 keV (demonstrated in a forthcoming publication [Tabet *et al.* unpublished]). Why this does not have a discernable effect on the relative production of fragment ions from uracil is an open question. The

* Allowing for errors associated primarily with corrections for ion acceptance, Gobet *et al.*'s [2004] proton impact data is in good agreement with the subsequent measurements carried out by Luna *et al.* [2007] in the impact energy range 20-100 keV.

relatively complex electronic configuration of uracil combined with the notoriously difficult theoretical treatment of ion-molecule interactions at *intermediate* velocities means that modeling the ionization processes observed in the present work represents a major challenge [Wang et al. *unpublished*].

In contrast to the electron capture results, energy dependence was observed in the relative production of uracil⁺ and fragment ions following direct ionization. In particular, at low impact energies (42-27 keV) table 2 shows a clear reduction in the relative production of uracil⁺ and of fragment ions belonging to the largest m/q group (the C₃H₃NO⁺ group), as well as increased relative production of H⁺. Hence an increase in direct ionization-induced dissociation was observed at lower proton impact energies. Between 50 and 150 keV, however, the present DI results do not provide clear evidence for impact energy dependence in the relative production of the different ion groups. Conversely, the energy dependence of the DI cross section for proton impact upon water [Gobet et al. 2001, 2004] or uracil [Tabet et al. *unpublished*] is weak in the lower energy part of the present range, whereas it becomes progressively more significant from 50 to 150 keV. Therefore, as with the electron capture data, the branching ratios shown in Fig. 5 for direct ionization cannot be explained adequately by a simple association of increased fragmentation with smaller impact parameters.

4. Conclusions

The first branching ratios for electron capture and direct ionization in proton-uracil collisions are presented as a function of impact energy in the range 20-150 keV (0.9-2.4 v₀). The impact energy dependence of the percentage of ionization events occurring through electron capture as opposed to direct ionization shows the same broad characteristics as observed for smaller molecules [Gobet et al. 2004, Luna et al. 2007, Rudd et al. 1983]. To the authors' knowledge, the present work provides the first comparison between molecular fragmentation following electron capture and direct ionization in proton collisions with a *relatively large* and electronically complex molecule; the only previous experiments of this kind were carried out on O₂ [Luna et al. 2005] and H₂O [Gobet et al. 2004, Luna et al. 2007]. No clear evidence was observed for energy-dependence in the relative production of uracil⁺ and fragment ions following electron capture, whereas a relative increase in fragment ion production was observed for direct ionization in the low impact energy part of the present range.

Acknowledgements

The *Institut de Physique Nucléaire de Lyon* is part of IN2P3-CNRS, the French national research institute for nuclear and particle Physics. Financial support was provided by the French, Austrian, and Moroccan governments, and the EU Commission (Brussels), through the Amadee and PICS 2290 programs, the CNRS-CNRST (n°17689) convention. S. Eden acknowledges the FP6 Marie Curie Fellowship (IEF RADAM-BIOCLUS)..

References

- R. Becker and G. Kogan, *Photochem. Photobiol.* **31** (1980) 5
- J. Berkowitz, J. P. Greene, H. Cho, and B. Ruscic, *J. Chem. Phys.* **86** (1987) 674
- M. Biaggi, F. Ballarini, W. Burkard, E. Egger, A. Ferrari, A. Ottolenghi, *Nucl. Instr. Methods Phys. Res. B* **159** (1999) 89
- B. Boudaiffa, P. Cloutier, D. Hunting, M.A. Hues, and L. Sanche, *Science* **287** (2000) 1658
- R. Cabrera-Trujillo, Y. Öhrn, E. Deumens, and J. R. Sabin, *Phys. Rev. A* **62** (2000) 052714
- R. Cabrera-Trujillo, P. Apell, J. Oddershede, and J. R. Sabin, *Application of Accelerators in Research and Industry International Conference: AIP Conference Proceedings* **680** (2003) 86
- M. Carré, M. Druetta, M. L. Gaillard, H. H. Bukow, M. Horani, A.L. Roche, and M. Velghe, *Mol. Phys.* **40** (1980) 1453
- B. Coupier, B. Farizon, M. Farizon, M. J. Gaillard, F. Gobet, N. V. de Castro Faria, G. Jalbert, S. Ouaskit, M. Carré, B. Gstyr, G. Hanel, S. Denifl, L. Feketeova, P. Scheier, and T. D. Märk, *Eur. Phys. J. D* **20** (2002) 459
- J. de Vries, R. Hoekstra, R. Morgenstern, and T. Schlathölter, *J. Phys. B: At. Mol. Opt. Phys.* **35** (2002) 4373
- J. de Vries, R. Hoekstra, R. Morgenstern, and T. Schlathölter, *Phys. Rev. Lett.* **91** (2003) 053401
- J. de Vries, R. Hoekstra, R. Morgenstern, and T. Schlathölter, *Physica Scripta* **T110** (2004) 336
- S. Denifl, B. Sonnweber, G. Hanel, P. Scheier, and T. D. Märk, *Int. J. Mass Spectrom.* **238** (2004) 47
- C. Desfrancois, H. Abdoul-Carime, and J. P. Schermann, *J. Chem. Phys.* **104** (1996) 7792
- S. Feil, K. Gluch, S. Matt-Leubner, P. Scheier, J. Limtrakul, M. Probst, H. Deutsch, K. Becker, A. Stamatovic, and T. D. Märk, *J. Phys. B* **37** (2004) 3013
- W. Friedland, P. Jacob, P. Bernhardt, H. G. Paretzke, and M. Dingfelder, *Radiat. Res.* **159** (2003) 401
- F. Gobet, B. Farizon, M. Farizon, M.J. Gaillard, M. Carre, M. Lezius, P. Scheier, and T.D. Märk, *Phys.*

- Rev. Lett.* **86** (2001) 3751
- F. Gobet, S. Eden, B. Coupier, J. Tabet, B. Farizon, M. Farizon, M. J. Gaillard, M. Carré, S. Ouaskit, T. D. Märk, and P. Scheier, *Phys. Rev. A* **70** (2004) 062716
- F. Gobet, S. Eden, B. Coupier, J. Tabet, B. Farizon, M. Farizon, M. J. Gaillard, S. Ouaskit, M. Carré, and T. D. Märk, *Chem. Phys. Lett.* **421** (2006) 68
- M. Imhoff, Z. Deng, and M. Huels, *Int. J. Mass Spectrom.* **245** (2005) 68
- M. Imhoff, Z. Deng, and M. Huels, *Int. J. Mass Spectrom.* **262** (2007) 154
- H. W. Jochims, M. Schwell, H. Baumgärtel, and S. Leach, *Chem. Phys.* **314** (2005) 263
- A. Le Padellec, P. Moretto-Capelle, M. Richard-Viard, J. P. Champeaux, and P. Cafarelli, *Journal of Physics: Conference Series* **101** (2008) 012007
- H. Luna, A. L. F. de Barros, J. A. Wyer, S. W. J. Scully, J. Lecointre, P. M. Y. Garcia, G. M. Sigaud, A. C. F. Santos, V. Senthil, M. B. Shah, C. J. Latimer, and E. C. Montenegro, *Phys. Rev. A* **75** (2007) 042711
- H. Luna, C. McGrath, M. B. Shah, R. E. Johnson, M. Liu, C. J. Latimer, and E. C. Montenegro, *The Astrophysical Journal* **628** (2005) 1086
- C. M. Marian, F. Schneider, M. Kleinschmidt, and J. Tatchen, *Eur. Phys. J. D* **20** (2002) 357
- P. Moretto-Capelle and A. Le Padellec, *Phys. Rev. A* **74** (2006) 062705
- NIST Chemistry WebBook available from <http://webbook.nist.gov>
- J. M. Rice, G. O. Dudek, and M. Barber, *J. Am. Chem. Soc.* **87** (1965) 4569
- M. E. Rudd, R. D. DuBois, L. H. Toburen, C. A. Ratcliffe, and T. V. Goffe, *Phys. Rev. A* **28** (1983) 3244
- T. Schlathölder, F. Alvarado, and R. Hoekstra, *Nucl. Instr. and Meth. in Phys. Res. B* **223** (2005) 62
- T. Schlathölder, F. Alvarado, S. Bari, A. Lecointre, R. Hoekstra, V. Bernigaud, B. Manil, J. Rangama, and B. Huber, *ChemPhysChem* **7** (2006) 2339
- O. V. Shishkin, L. Gorb, A.V. Luzanov, M. Elstner, S. Suhai, and J. Leszczynski, *J. Mol. Structure* **625** (2003) 295
- K. B. Snow and T. F. Thomas, *Int. J. Mass Spectrom. Ion Processes* **96** (1990) 49
- J. Tabet, S. Eden, S. Feil, H. Abdoul-Carime, B. Farizon, M. Farizon, S. Ouaskit, and T. D. Märk, *unpublished*
- C. von Sonntag, *The Chemical Basis for Radiation Biology*, Taylor and Francis, London, 1987
- B. Walch, C. L. Cocke, R. Voepel, and E. Salzborn, *Phys. Rev. Lett.* **72** (1994) 1439

W. C. Wiley and I. H. McLaren, *Rev. Sci. Instrum.***16** (1955) 1150

Z. P. Wang, P. M. Dinh, P.-G. Reinhard, E. Suraud, G. Bruny, C. Montano, S. Feil, S. Eden, H.

Abdoul-Carime, B. Farizon, M. Farizon, S. Ouaskit, and T. D. Märk, *unpublished*

Fig. 1: Electron capture ionization of uracil as a percentage of total ionization (electron capture + direct ionization) following proton impact in the energy range 27-150 keV. Dark line: exponential fit. Insert: schematic representation of the structure of the uracil.

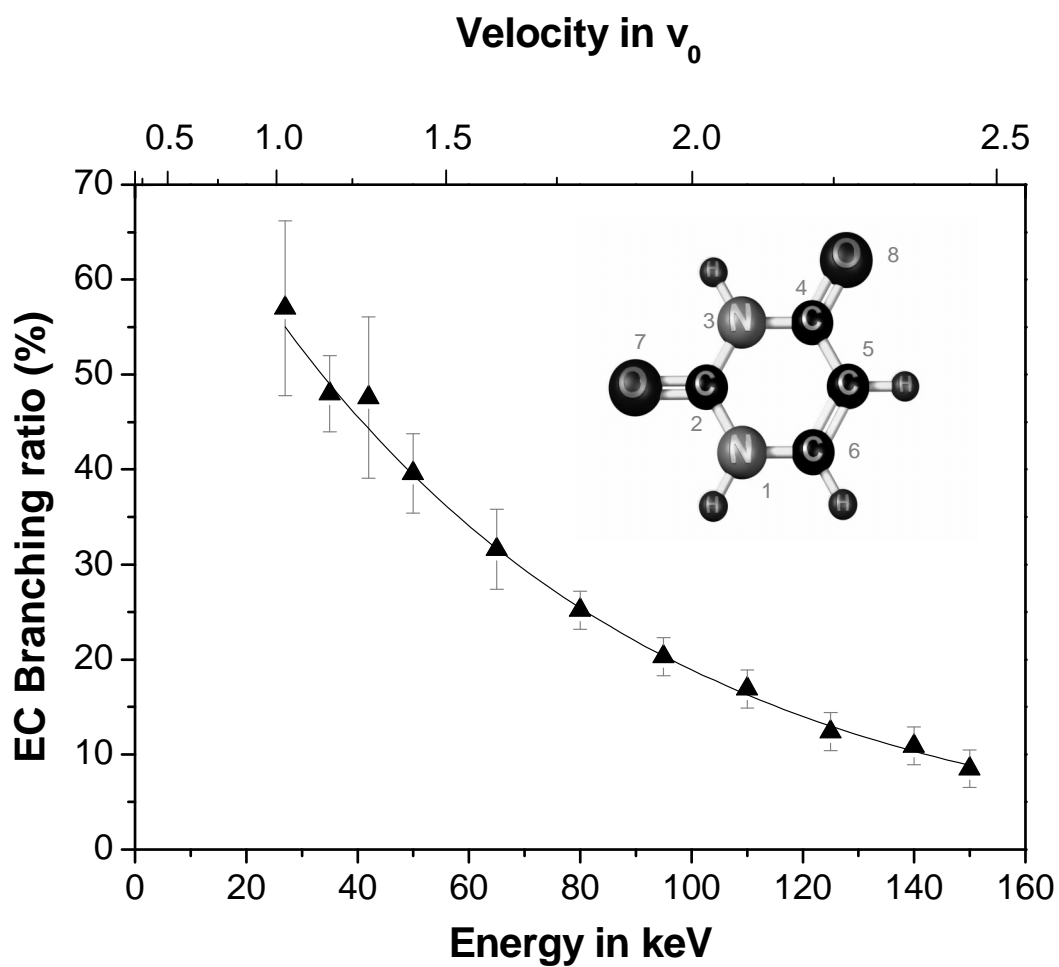


Fig. 2: Schematic diagram of the experimental system

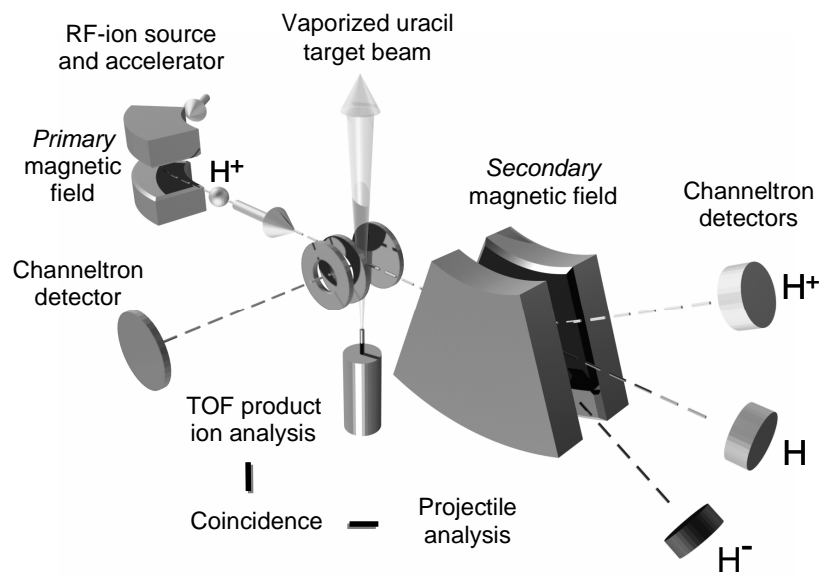


Fig. 3: Electron capture ionization of uracil as a percentage of total ionization (electron capture + direct ionization) following proton impact in the energy range 27-150 keV. The data is compared to previous results for H₂O [Gobet *et al.* 2004, Luna *et al.* 2007], and for He, CH₄, CO₂, and O₂ [Rudd *et al.* 1983].

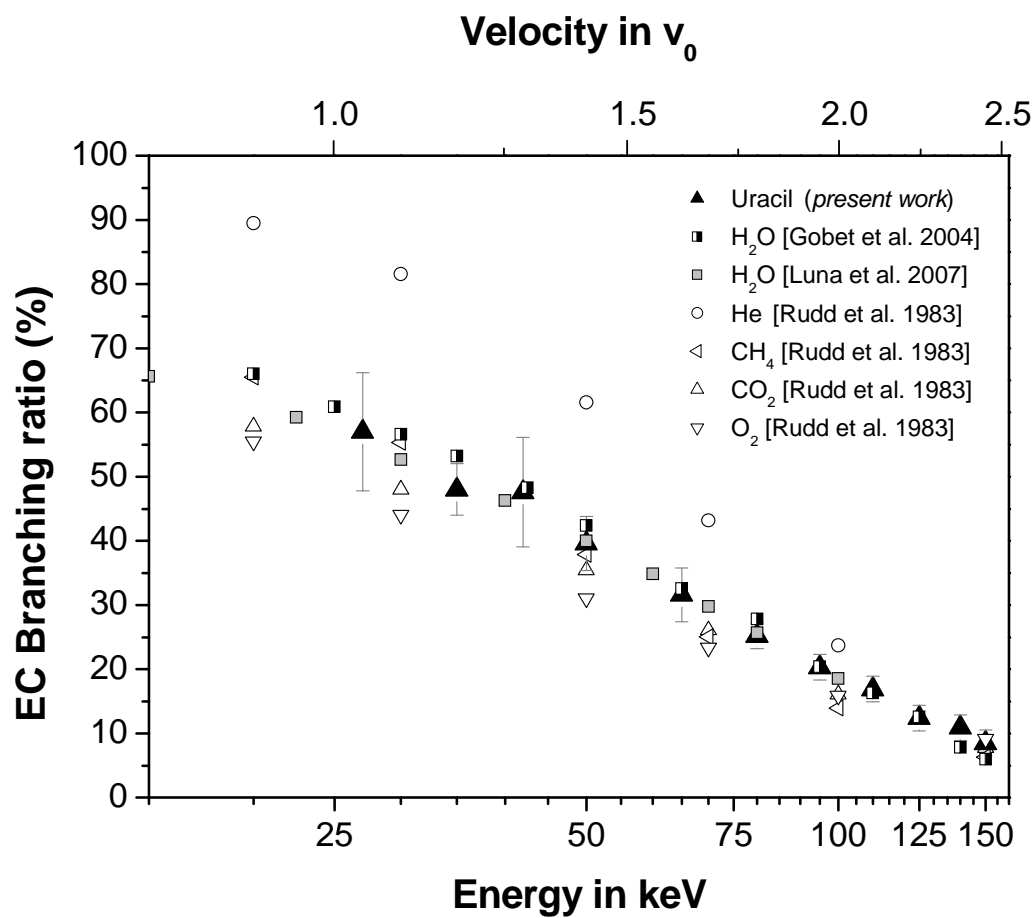


Fig. 4: Mass spectrum for the proton impact ionization of uracil ($C_4H_4N_2O_2$, 112 amu) by electron capture and by direct ionization at 80 keV. The principle ions expected to account for the peaks are listed in table 1.

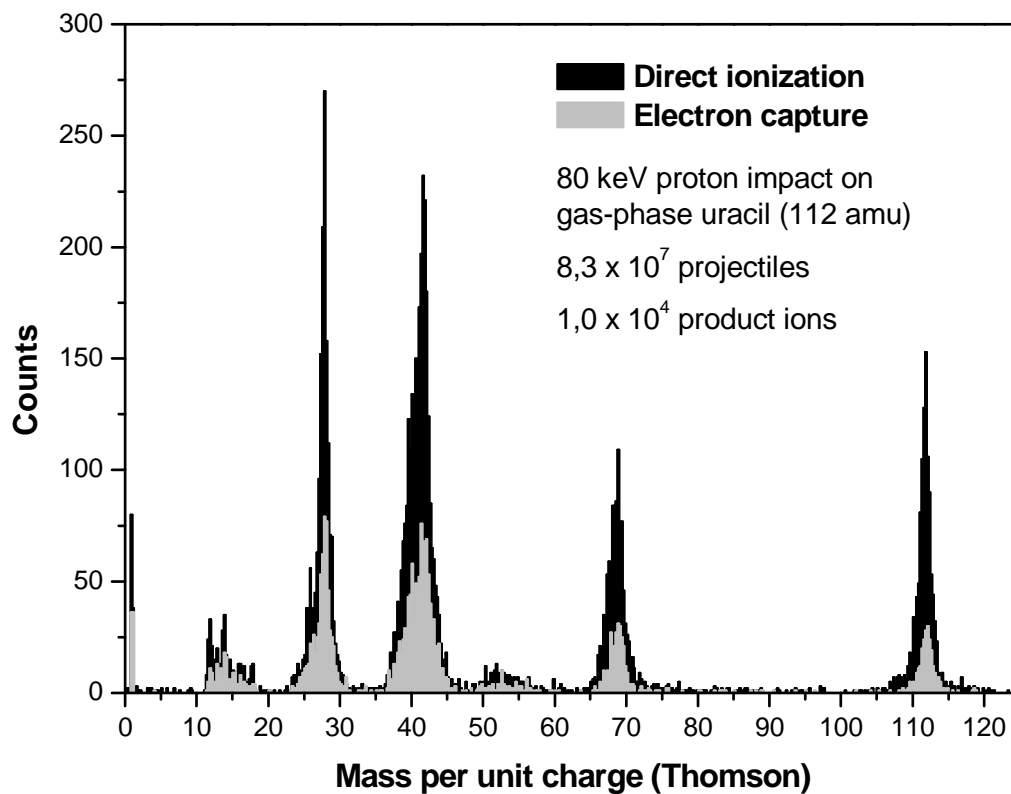
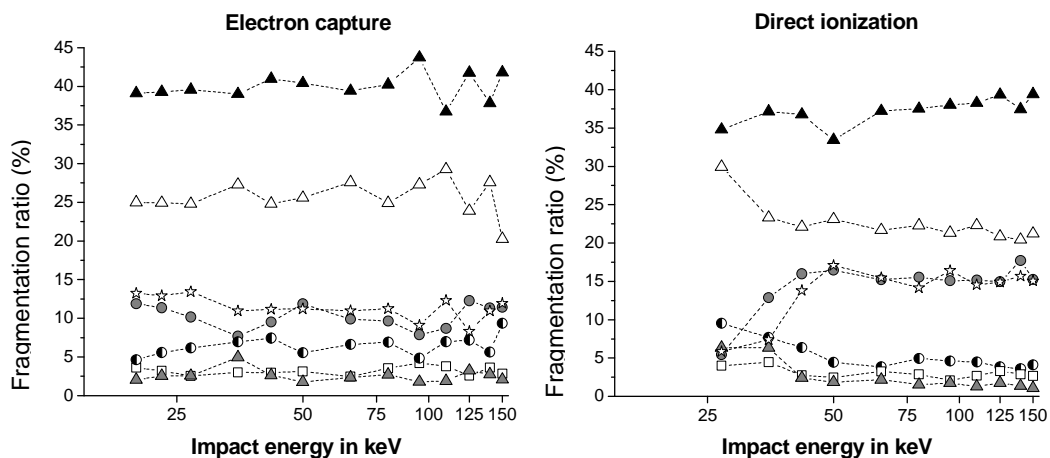


Figure 5: Product ion percentage branching ratios (the number of ions detected in a given mass range over the total number of ions detected) in 20-150 keV proton collisions with uracil. Background noise has been removed and ions produced by electron capture and by direct ionization are treated separately. Dashed lines have been added to guide the eye and statistical errors are given in table 2.



Grey filled circles = uracil⁺ peak (half-max. width 111-112 Thomson); open stars = C₃H₃NO⁺ group (half-max. width 67-69); open squares = C₂H₂NO⁺ group (half-max. width 50-56); black filled triangles = CNO⁺ / C₂H₄N⁺ / C₂H₂O⁺ group (half-max. width 39-43); open triangles = CH₂N⁺ group (half-max. width 27-28); half-filled circles = CH₂⁺ group (full range 12-18); grey filled triangles = H⁺ peak.

Table 1: Product ions observed following the ionization of gas-phase uracil ($C_4H_4N_2O_2$) by photons [Jochims *et al.* 2005], by fast incident protons (present work) and by electrons [Imhoff *et al.* 2007, Denifl *et al.* 2004]. The desorbed cations observed for slow Ar^+ impact upon condensed phase uracil are also listed [Imhoff *et al.* 2007].

<i>m/z</i> (with previous fragment ion proposals)					
200 eV Ar^+ impact on condensed uracil Imhoff <i>et al.</i> [2007]	Gas-phase uracil ionization				
	70 eV electron impact		20 eV photo-ionization Jochims <i>et al.</i> [2005] ^B	100 keV proton impact Le Padellec <i>et al.</i> [2007] ^C	Present work: 20-150 keV proton impact ^{D, E, F}
	Imhoff <i>et al.</i> [2007]	Denifl <i>et al.</i> [2004] ^A			
114					
113 (Uracil + H) ⁺	113				
112 (Uracil ⁺)	112 (Uracil ⁺)	112 (Uracil ⁺)	112 (Uracil ⁺)	112	111-112 (peak 112)
97 ($C_4H_5N_2O^+$)					
96 ($C_4H_4N_2O^+$)			96 ($C_4H_4N_2O^+$) - weak		
95 ($C_4H_3N_2O^+$)					
71					
70 ($C_3H_4NO^+$)	70 ^G ($C_3H_4NO^+$)		70 ($C_3H_4NO^+$) - weak		67-69 (peak 69)
69 ($C_3H_3NO^+$)	69 ($C_3H_3NO^+$)	69 ($C_3H_3NO^+$)	69 ($C_3H_3NO^+$)	69	
68 ($C_3H_2NO^+$)	68 ($C_3H_2NO^+$)	68 ($C_3H_2NO^+$)	68 ($C_3H_2NO^+$)	68	
	67				
56	56	56 ($C_2H_2NO^+$ / CN_2O^+)	56 - weak	56*	
55	55				
54	54			54*	
53	53		53 - weak	53*	
52	52		52 - weak	52*	
51	51			51*	
45					
44 (CH_2NO^+)	44 (CH_2NO^+)		44 - weak	44	
43	43	43 ($CHNO^+$)	43 ($CHNO^+$)	43	
42 ($C_2H_4N^+$)	42 ($C_2H_4N^+$)	42 (CNO^+)	42 ($C_2H_2O^+$)	42	
41 ($C_2H_3N^+$)	41 ($C_2H_3N^+$)	41 (C_2HO^+ / $C_2H_3N^+$)	41 (C_2HO^+ / $C_2H_3N^+$)	41	
40 ($C_2H_2N^+$)	40 ($C_2H_2N^+$)		40 ($C_2H_2N^+$)	40	
39	39		39 - weak	39*	
38	38			38	
30	30				
29	29		29 (CH_3N^+ / HCO^+) - weak	29	
28 (CH_2N^+)	28 (CH_2N^+ / CO^+)	28 (CH_2N^+ / CO^+)	28 (CH_2N^+)	28 (CH_2N^+ / CO^+)	27-28 (peak 28)
27	27	27 (CHN^+)	27 (CHN^+) - weak	27*	
26 ($C_2H_2^+$)	26 ($C_2H_2^+$)		26 ($C_2H_2^+$) - weak	26*	
25	25			25*	
18	18		18 (H_2O^+ impurity) - weak	18*	
17	17		17 (NH_3^+) - weak	17 (OH^+)	
16	16			16*	
15 (CH_3^+)	15 (CH_3^+)			15 (NH^+)	
14 (CH_2^+)	14 (CH_2^+)	Not available	14 (N^+) - weak	14 (N^+)	
13	13			13 (CH^+)	
12	12			12 (C^+)	
	2		Not available	Not available	
1 (H^+)	1 (H^+)				1

^A This column only includes the masses tabulated in the work of Denifl *et al.* [2004]; other trace ions are visible in the published mass spectrum.

^B The photo-ionization channels labeled *weak* correspond to those reported by Jochims *et al.* [2005] to have intensities $\leq 5\%$ of the maximum peak intensity (42 amu).

^C The non-asterisked product ion masses were labeled or mentioned explicitly by Le Padellec *et al.* [2004]. Conversely, the asterisked masses have been taken from a published figure and are therefore subject to greater uncertainty.

^D The same product ion groups and peak positions were observed for both direct ionization and electron capture across the full proton impact energy range studied (20-150 keV).

^E With the exception of 12-18 (the full range of the group), the ranges given in the *present data* column correspond to the half-maximum width of the 80 keV DI peaks.

^F The present data only includes single ion production.

^G Imhoff *et al.* [2007] also suggested that $C_3H_3NO^+$ including a ^{13}C isotope may contribute to this peak.

Table 2: Product ion fragmentation ratios (the number of ions detected in a given mass range over the total number of ions detected) in % for 20-150 keV proton collisions with uracil. Background noise has been removed and ions produced by direct ionization and by electron capture are treated separately.

Impact energy (keV)	Fragment ion production / total ionization (%)													
	H ⁺		CH ₂ ⁺ group (12-18) ^A		CH ₂ N ⁺ group (27-28) ^B		CNO ⁺ / C ₂ H ₄ N ⁺ / C ₂ H ₂ O ⁺ group (39-43) ^B		C ₂ H ₂ NO ⁺ group (50-56) ^B		C ₃ H ₃ NO ⁺ group (67-69) ^B		uracil ⁺ (111-112) ^B	
	EC	DI	EC	DI	EC	DI	EC	DI	EC	DI	EC	DI	EC	DI
20	2.1 ± 0.4	-	4.6 ± 0.6	-	25.0 ± 1.4	-	39.1 ± 1.9	-	3.6 ± 0.5	-	13.2 ± 1.0	-	11.9 ± 0.9	-
23	2.6 ± 0.5	-	5.6 ± 0.8	-	24.9 ± 1.8	-	39.3 ± 2.4	-	3.2 ± 0.6	-	12.9 ± 1.2	-	11.4 ± 1.1	-
27	2.6 ± 0.4	6.4 ± 2.7	6.2 ± 0.6	9.6 ± 4.4	24.8 ± 1.3	29.9 ± 8.4	39.6 ± 1.7	34.8 ± 7.6	2.5 ± 0.4	4.0 ± 2.8	13.4 ± 0.9	5.9 ± 3.1	10.2 ± 0.7	5.5 ± 2.7
35	5.0 ± 0.6	6.4 ± 3.4	6.9 ± 0.8	7.7 ± 4.8	27.3 ± 1.6	23.3 ± 8.4	39.0 ± 2.0	37.2 ± 10.2	3.0 ± 0.5	4.5 ± 3.3	11.0 ± 0.9	7.4 ± 4.0	7.7 ± 0.7	12.9 ± 4.7
42	2.7 ± 0.4	2.4 ± 1.8	7.4 ± 0.6	6.4 ± 3.0	24.8 ± 1.2	22.1 ± 5.5	41.0 ± 1.6	36.8 ± 6.7	3.0 ± 0.4	2.8 ± 2.0	11.2 ± 0.7	13.8 ± 3.6	9.5 ± 0.7	16.0 ± 3.6
50	1.8 ± 0.4	1.9 ± 0.9	5.5 ± 0.7	4.5 ± 1.3	25.6 ± 1.8	23.1 ± 2.8	40.4 ± 2.2	33.5 ± 2.6	3.1 ± 0.5	2.5 ± 0.9	11.2 ± 1.0	17.1 ± 2.2	11.9 ± 1.1	16.5 ± 2.0
65	2.4 ± 0.5	2.2 ± 0.6	6.6 ± 0.8	3.9 ± 0.7	27.6 ± 1.7	21.7 ± 1.7	39.4 ± 2.2	37.2 ± 1.6	2.5 ± 0.5	3.3 ± 0.6	11.0 ± 1.0	15.5 ± 1.3	9.9 ± 1.0	15.2 ± 1.2
80	2.7 ± 0.3	1.5 ± 0.3	6.9 ± 0.6	5.0 ± 0.5	24.9 ± 1.1	22.3 ± 1.0	40.2 ± 1.5	37.5 ± 1.0	3.6 ± 0.4	2.9 ± 0.3	11.2 ± 0.7	14.2 ± 0.7	9.6 ± 0.7	15.5 ± 0.7
95	1.8 ± 1.0	1.7 ± 0.8	4.8 ± 1.8	4.6 ± 1.2	27.3 ± 4.7	21.3 ± 2.5	43.7 ± 6.3	38.0 ± 2.3	4.2 ± 1.7	2.1 ± 0.8	9.1 ± 2.5	16.4 ± 2.1	7.9 ± 2.3	15.1 ± 1.9
110	1.9 ± 0.7	1.3 ± 0.5	7.0 ± 1.3	4.5 ± 0.7	29.3 ± 2.9	22.3 ± 1.5	36.7 ± 3.3	38.3 ± 1.5	3.8 ± 0.9	2.7 ± 0.5	12.3 ± 1.7	14.6 ± 1.1	8.7 ± 1.4	15.2 ± 1.1
125	3.2 ± 0.9	1.8 ± 0.5	7.2 ± 1.4	3.9 ± 0.6	23.9 ± 2.7	20.9 ± 1.4	41.8 ± 3.8	39.3 ± 1.5	2.6 ± 0.8	3.3 ± 0.5	8.3 ± 1.5	14.9 ± 1.1	12.3 ± 1.8	15.0 ± 1.0
140	2.8 ± 0.8	1.4 ± 0.4	5.6 ± 1.2	3.6 ± 0.6	27.6 ± 2.8	20.4 ± 1.3	37.8 ± 3.4	37.5 ± 1.4	3.6 ± 0.9	2.9 ± 0.5	10.9 ± 1.7	15.7 ± 1.0	11.3 ± 1.7	17.7 ± 1.0
150	2.1 ± 0.7	1.1 ± 0.3	9.4 ± 1.6	4.1 ± 0.5	20.3 ± 2.5	21.3 ± 1.1	41.8 ± 3.9	39.4 ± 1.2	2.9 ± 0.9	2.7 ± 0.4	11.9 ± 1.9	15.1 ± 0.9	11.4 ± 1.8	15.3 ± 0.8

^A Unlike the other product ion groups, this group contains more than one peak. The group is named after CH₂⁺, associated with the lower mass peak in the product ion group. 12-18 Thomson is the full m/q range of the group (see also figure 4 and table 1)

^B The m/q values in brackets correspond to the half-maximum width of each product ion group. The groups are named after the principle ion associated with the peak [Jochims *et al.* 2005, Imhoff *et al.* 2007, Denifl *et al.* 2004].

The errors given in the table are purely statistical; variations in the detection efficiency of different ions due to the acceptance of the TOF mass spectrometer have not been taken into account.